Predictive control for RIS-aided B5G networks using Kalman filters

Rafael Marasca Martins, Luis Carlos Mathias, and Taufik Abrão

***Abstract*— Reconfigurable Intelligent Surfaces (RIS) are a key enabler for B5G/6G wireless networks, particularly in dense urban environments, enhancing spectral efficiency through controlled signal propagation. However, accurate User Equipment (UE) tracking is essential for real-time RIS reconfiguration, especially in scenarios where the system depends on low-rate, noisy Global Positioning System (GPS) updates. To address this, we propose a Kalman filter-based control algorithm that estimates the UE's position between GPS samples, allowing the RIS to optimize received power. Results show that this method can boost received power fivefold, demonstrating its effectiveness as a low-complexity solution for real-time beamforming in mobile scenarios with sparse location data.**

***Keywords*— RIS, Kalman filter, Predictive control, B5G, 6G.**

I. Introduction

One of the greatest challenges in modern communications within dense urban environments is overcoming multipath fading, which arises from signal reflections and attenuation caused by interactions with the surrounding environment, such as building foundations, metal structures, and other obstacles [1], [2]. In this context, Intelligent Reflecting Surfaces (RIS) emerge as a promising enabling technology, as they can make the propagation environment controllable by passively and electronically adjusting the phase of reflected signals [1]–[3]. This capability allows RIS to create constructive or destructive interference in specific spatial regions, enhancing signal quality where needed. Another important advantage of RIS is its ability to mitigate shadowing by creating a virtual Line-of-Sight (LoS) between the Base Station (BS) and the User Equipment (UE) [1], [3].

However, a key requirement of Beyond 5G (B5G) and 6G networks is Ultra-Reliable Low-Latency Communication (URLLC) [3], [4]. This imposes strict constraints on the control algorithms, which must operate with minimal latency to reduce the overhead during the RIS reconfiguration phase—particularly the communication delays between the UE, BS, and RIS. Therefore, minimizing this reconfiguration overhead is critical for ensuring high Quality of Service (QoS), especially for mobile users [2], [3].

However, when a precise and high-rate sensing infrastructure is not available, the adjustment of the RIS must rely on low-rate and noisy Global Positioning System (GPS) measurements of the UE's position. But, as the wireless communication channel is intrinsically stochastic and highly volatile, mainly due to factors such as weather changes, user mobility, and the dynamic presence of obstacles [1], the RIS is unable to accurately reconfigure itself to track the UE's position adequately, resulting in degraded beam alignment and reduced communication performance [2]. This highlights the need for predictive control strategies capable of estimating the UE's trajectory in real time, even with sparse and uncertain measurements.

Several works, such as [5] and [6], explore Integrated Sensing and Communications (ISAC) techniques; however, their applicability can be limited by power, throughput, or interference constraints [7]. As a complementary direction, [8] proposes a transformer-based method that fuses camera and GPS data to predict beam states up to 500 ms in advance, enhancing received power. Nevertheless, this approach relies heavily on large volumes of data, which may not always be practical. Similarly, [9] presents an unsupervised clustering algorithm to estimate the true vehicle trajectory from sparse and noisy GPS data. While effective, these machine learning–based, data-centric solutions depend on substantial training data, which may limit their deployment in real-world scenarios.

A promising solution lies in the use of the Kalman filter. By leveraging past observations and a motion model, the Kalman filter provides optimal estimates of the system state, making it particularly well-suited for real-time tracking and prediction in dynamic environments such as mobile wireless networks [10]. In this context, the present work proposes a predictive control algorithm based on Kalman filtering, which uses low-rate GPS measurements from a mobile UE to estimate its position between samples. These predictions enable proactive RIS reconfiguration that compensates for control latency and anticipates the UE's movement, ultimately improving received signal power. This approach aims to maintain high communication performance while avoiding power loss penalties of reactive reconfiguration.

II. Kalman Filter

The Kalman filter is a recursive algorithm widely used for estimating the state of dynamic systems. It operates in two main steps: prediction and update [10], [11].

The prediction step estimates the current system state $\mathbf{s}_i$ and its associated uncertainty based on the previous state, assuming a linear system model with additive Gaussian process noise. The underlying system dynamics are described by [10]–[12]:

$$\mathbf{s}_i = \mathbf{F}\mathbf{s}_{i-1} + \mathbf{w}_{i-1}, \quad \mathbf{w}_{i-1} \sim \mathcal{N}(\mathbf{0}, \mathbf{Q}) \tag{1}$$

where $\mathbf{s}_i$ is the state at time step i, $\mathbf{F}$ is the state transition matrix, and $\mathbf{w}_{i-1}$ is the process noise with covariance matrix

This study was financed in part by the Coordenação de Aperfeiçoamento de Pessoal de Nível Superior – Brasil (CAPES) – Finance Code 001.

R. Martins and T. Abrão are with the Department of Electrical Engineering, State University of Londrina (UEL), Londrina, PR, Brazil.

L. Mathias is with the Department of Computer Engineering, Federal University of Technology – Parana (UTFPR), PR, Brazil.

$\mathbf{Q}$. Based on this model, the predicted state estimate $\hat{\mathbf{s}}_i$ and its associated error covariance matrix $\widehat{\mathbf{P}}_i$ is computed as follows [10]–[12]:

$$\widehat{\mathbf{s}}_i = \mathbf{F}\mathbf{s}_{i-1} \tag{2}$$

$$\widehat{\mathbf{P}}_i = \mathbf{F}\mathbf{P}_{i-1}\mathbf{F}^T + \mathbf{Q} \tag{3}$$

where the notation $\widehat{(\cdot)}$ stands for the predicted estimate before the measurement update, and ^{T} represents the transpose of a vector or matrix. The update step is triggered when a new measurement is available. This step refines the predicted state using new information. It starts by computing the innovation covariance matrix $\mathbf{S}$ [10]–[12]:

$$\mathbf{S} = \mathbf{H}\mathbf{P}_i\mathbf{H}^T + \mathbf{R} \tag{4}$$

where $\mathbf{H}$ is the observation matrix that maps the predicted state to the measurement space, and $\mathbf{R}$ is the measurement noise covariance matrix, representing sensor uncertainties.

Next, the Kalman gain acts as a weighting factor that determines the relative importance of the measurement versus the prediction. It is denoted by $\mathbf{G}$ and can be calculated as follows [10]–[12]:

$$\mathbf{G} = \widehat{\mathbf{P}}_i\mathbf{H}^T\mathbf{S}^{-1} \tag{5}$$

The residual vector $\mathbf{e}_i$, representing the difference between the actual UE position measurement $\mathbf{r}_i$ and the predicted measurement, is given by [11]:

$$\mathbf{e}_i = \mathbf{r}_i - \mathbf{H}\widehat{\mathbf{s}}_i \tag{6}$$

The actual state and its covariance are then updated as follows [10]–[12]:

$$\mathbf{s}_i = \widehat{\mathbf{s}}_i + \mathbf{G}\mathbf{e}_i \tag{7}$$

$$\mathbf{P}_i = (\mathbf{I} - \mathbf{G}\mathbf{H})\widehat{\mathbf{P}}_i \tag{8}$$

A. System Model

In this paper, two motion models are considered to describe the system dynamics: a constant acceleration (CA) model and a constant velocity (CV) model. Accordingly, the state vectors for each model are defined as follows:

$$\mathbf{s}_{\text{CA}} = \begin{bmatrix} x & \dot{x} & \ddot{x} & y & \dot{y} & \ddot{y} & z & \dot{z} & \ddot{z} \end{bmatrix}^T \tag{9}$$

$$\mathbf{s}_{\text{CV}} = \begin{bmatrix} x & \dot{x} & y & \dot{y} & z & \dot{z} \end{bmatrix}^T \tag{10}$$

where x, y, and z denote the coordinates of the UE; $\dot{x}$, $\dot{y}$, and $\dot{z}$ denote the corresponding velocity components; and $\ddot{x}$, $\ddot{y}$, and $\ddot{z}$ represent the acceleration components (included only in the CA model).

The Kalman filter's state vector is initialized using the first available GPS measurement, under the assumption that the UE starts from rest. That is, all initial velocities and accelerations are set to zero at the beginning of the estimation process.

Based on the classical kinematic equations of motion, the system state can be extrapolated over a time interval Δt under the CV or CA assumption. These equations form the basis for the state transition models employed in this work, which are derived based on [10], [12].

Constant Acceleration Model: In the CA model, the position, the corresponding state transition matrix $\mathbf{F}_{\text{CA}}$ for the full 9-dimensional state vector is:

$$\mathbf{F}_{\text{CA}} = \mathbf{I_3} \otimes \begin{bmatrix} 1 & \Delta t & \frac{1}{2}\Delta t^2 \\ 0 & 1 & \Delta t \\ 0 & 0 & 1 \end{bmatrix} \tag{11}$$

where $\otimes$ denotes the Kroenecker product.

Constant Velocity Model: In the CV model, the system assumes no acceleration; therefore, the position changes linearly with velocity, and velocity remains constant. Thus, the corresponding 6-dimensional state transition matrix $\mathbf{F}_{\text{CV}}$ is [12]:

$$\mathbf{F}_{\text{CV}} = \mathbf{I_3} \otimes \begin{bmatrix} 1 & \Delta t \\ 0 & 1 \end{bmatrix} \tag{12}$$

These transition matrices are used in the prediction step of the Kalman filter to estimate the next state based on the current state and the underlying motion model.

B. Covariance Matrices

Assuming the estimation errors across the x, y, and z axes are uncorrelated, the initial error covariance matrix $\mathbf{P}$ and process noise covariance matrix $\mathbf{Q}$ are structured in a block-diagonal form.

Error Covariance Matrix: The error covariance matrix $\mathbf{P}$ follows the general definition [11], [12]:

$$\mathbf{P} = \mathbb{E}\{\mathbf{s}\mathbf{s}^T\} \tag{13}$$

For both the CV and CA models, $\mathbf{P}$ is block-diagonal per axis:

$$\mathbf{P} = \begin{bmatrix} \mathbf{P}_x & \mathbf{0} & \mathbf{0} \\ \mathbf{0} & \mathbf{P}_y & \mathbf{0} \\ \mathbf{0} & \mathbf{0} & \mathbf{P}_z \end{bmatrix} \tag{14}$$

Here, $\mathbf{0}$ denotes a zero matrix of appropriate dimensions, and each $\mathbf{P}_k$ ($k \in \{x, y, z\}$) is a square matrix of size $q \times q$, where $q = 2$ for the CV model and $q = 3$ for the CA model:

$$\mathbf{P}_k = \begin{cases} \begin{bmatrix} p_{kk} & p_{k\dot{k}} \\ p_{\dot{k}k} & p_{\dot{k}\dot{k}} \end{bmatrix}, & \text{CV model} \\ \\ \begin{bmatrix} p_{kk} & p_{k\dot{k}} & p_{k\ddot{k}} \\ p_{\dot{k}k} & p_{\dot{k}\dot{k}} & p_{\dot{k}\ddot{k}} \\ p_{\ddot{k}k} & p_{\ddot{k}\dot{k}} & p_{\ddot{k}\ddot{k}} \end{bmatrix}, & \text{CA model} \end{cases}$$

The initial covariance matrix is typically initialized with high variances to reflect uncertainty, especially in velocity and acceleration states.

Process Noise Covariance Matrix: The process noise covariance matrix $\mathbf{Q}$ captures the uncertainty introduced by the system dynamics and is derived by projecting the continuous-time noise model $\mathbf{Q}_c$ through the system transition matrix $\mathbf{F}$ [11]:

$$\mathbf{Q} = \mathbf{F}\mathbf{Q}_c\mathbf{F}^\top \tag{15}$$

In the constant acceleration model, the process noise is typically attributed to random perturbations in acceleration, which propagate into both velocity and position. In contrast, the constant velocity model assumes that only the velocity component is affected by noise.

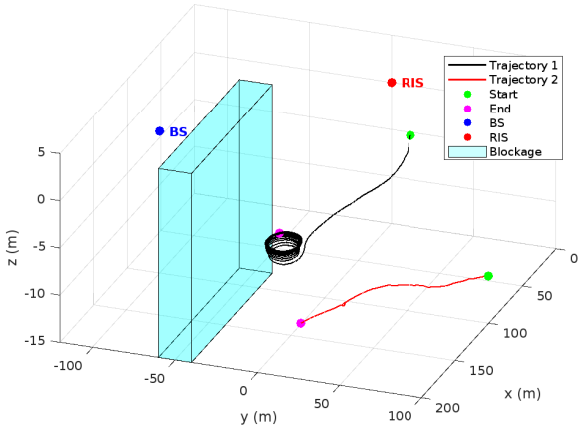

Fig. 1. Trajectories of the UE extracted from real datasets

C. Measurement Model

In the proposed system, each measurement corresponds to the UE's Cartesian position relative to the RIS. Therefore, the measurement matrix $\mathbf{H}$ maps the full state vector to the observed position components. It effectively selects the position entries (x, y, z) from the state vector while ignoring the unobserved velocity and acceleration states.

Assuming uncorrelated errors across dimensions, the measurement noise covariance matrix $\mathbf{R}$ is:

$$\mathbf{R} = \begin{bmatrix} \sigma_x^2 & 0 & 0 \\ 0 & \sigma_y^2 & 0 \\ 0 & 0 & \sigma_z^2 \end{bmatrix} \tag{16}$$

where σ_x^2, σ_y^2, and σ_z^2 denote the measurement variances along each axis.

In the remainder of this paper, we adopt the CA model as the default state-space formulation for the Kalman filter. Therefore, unless otherwise specified, all references to Kalman filter pertain to the CA model.

III. Methodology

The system considered in this paper comprises a fixed BS located at position $[100, -100, 0]$ m, a RIS at $[0, 0, 0]$ m, and a UE allowed to move freely within a defined area. We assume that, throughout the UE's trajectory, a physical obstacle obstructs the LoS path between the BS and the UE as depicted in Fig. 1. Both the UE and BS are equipped with isotropic antennas.

To simulate realistic vehicular motion, we employ two trajectories sourced from real-world GPS datasets. The first (Trajectory 1) is taken from [13], which contains 10 Hz GPS samples collected from various cars and drivers operating on public roads across the United Kingdom, Nigeria, and France. The second (Trajectory 2) comes from [14], featuring 1 Hz tracking data of South African minibus taxis, capturing dynamic driving behaviors such as aggressive acceleration. To enable quasi-continuous system evaluation, these signals are upsampled to 100 Hz via linear interpolation, which is sufficient given the relatively smooth nature of the underlying movements.

In addition to the empirical trajectories, a synthetic scenario (trajectory 3) is evaluated through a Monte Carlo simulation with 100 repetitions. Here, the UE follows a simulated path generated by a random-walk process in acceleration. At each time step, the position is updated using the kinematic equations:

$$\begin{cases} \mathbf{r}_t = \mathbf{r}_{t-1} + \dot{\mathbf{r}}_{t-1}\Delta t + 0.5\ddot{\mathbf{r}}\Delta t^2, \\ \dot{\mathbf{r}}_t = \dot{\mathbf{r}}_{t-1} + \ddot{\mathbf{r}}\Delta t \end{cases} \tag{17}$$

where the acceleration $\ddot{\mathbf{r}}_t$ at each time step is independently drawn from a Gaussian distribution with zero mean and variance 0.1 m/s^2. Both the initial position and velocity are assumed to be zero. This formulation enables a wide range of motion patterns.

The UE's trajectory is estimated in real time using a Kalman filter based on a constant acceleration motion model, and a Kalman filter based on the constant velocity model. These filters operate with a dual-rate structure: a high-frequency prediction step and a low-frequency update step. The prediction step is executed every 10 ms, producing rapid estimates of the UE's position, velocity, and acceleration, which are used to continuously adjust the RIS configuration for optimal signal reflection. Conversely, the update step occurs only when new GPS data is received, reflecting the sampling rate of the source. During this step, the filter refines its internal state by incorporating the new measurement, thereby correcting any accumulated drift.

For each predicted state, the phase shift that maximizes the received power at the UE can be determined for each RIS element as [15]:

$$\angle\Gamma_{m,n} = \mathrm{mod}\left(k_0\left(|r^{\mathrm{tx}}_{m,n}| + |\hat{r}^{\mathrm{rx}}_{m,n}|\right), 2\pi\right) \tag{18}$$

where $|r^{\mathrm{tx}}_{m,n}|$ and $|\hat{r}^{\mathrm{rx}}_{m,n}|$ are the exact distance from the BS and the estimated distance from the UE, respectively, to the (m,n)-th RIS element. If correctly estimated $|\hat{r}^{\mathrm{rx}}_{m,n}|$, the phase shifts obtained by (18) maximize the received power by allowing total constructive interference at the UE position.

The channel is modeled using a basic path-loss model, where the received power is given by Eq. 19 [15].

$$P_r = \frac{P_t\lambda^2}{(4\pi)^2}\sum_{m=1}^{M}\sum_{n=1}^{N}\frac{G_t(\theta^{\mathrm{tx}}_{m,n})G_r(\theta^{\mathrm{rx}}_{m,n})\sigma(\theta^t_{m,n},\theta^r_{m,n})|\Gamma_{m,n}|^2}{|r^{\mathrm{tx}}_{m,n}|^2|r^{\mathrm{rx}}_{m,n}|^2} \times e^{-2j\angle\Gamma_{m,n}+jk_0(|r^{\mathrm{tx}}_{m,n}|+|r^{\mathrm{rx}}_{m,n}|)} \tag{19}$$

In which P_t denotes the transmit power, λ is the signal wavelength, and G_t and G_r represent the transmit and receive antenna gains, respectively, both assumed to be 1 due to isotropic radiation. The RIS comprises M vertical and N horizontal elements. The angles $\theta^t_{m,n}$ and $\theta^r_{m,n}$ correspond to the angles of incidence and reflection at the (m,n)-th RIS element, while $|r^{\mathrm{rx}}_{m,n}|$ is the exact distance between the UE and the (m,n)-th RIS element. The radar cross-section of a unit cell, denoted by σ, is given by [15]:

$$\sigma(\theta^t_{m,n},\theta^r_{m,n}) = 4\pi\left(\frac{D^2}{\lambda}\right)^2\cos^2(\theta^t_{m,n}) \times\left(\frac{\sin\left(\frac{kD}{2}(\sin\theta^r_{m,n}-\sin\theta^t_{m,n})\right)}{\frac{kD}{2}(\sin\theta^r_{m,n}-\sin\theta^t_{m,n})}\right)^2 \tag{15}$$

where D is the periodicity of the elements, which is taken as $\lambda/2$ in this work.

IV. Numerical Results

This section compares the performance of the Kalman filter-based RIS configuration strategy with a naive approach, which reconfigures the RIS only when a new GPS coordinate is provided. The comparison is based on the received power at the UE, evaluated over time and under different sampling rates (1 Hz, 5 Hz, and 10 Hz). Figures 2, 3, and 4 illustrate the instantaneous power received at the UE for the three different employed trajectories (Fig. 4 represents the data from a single sample of the Monte Carlo simulation). Table I summarizes each condition's average power gain (in dB).

TABLE I
Comparison of Power Gain [dB] in UE for Different Methods and Sampling Rates for Three Trajectories

Trajectory	Method	Sampling Rate (Hz)		
		1Hz	5Hz	10Hz
Trajectory 1	Kalman	-0.3290	-0.3462	-0.0454
	Kalman (CV)	-0.3707	-0.2875	-0.2542
	Naive	-1.5868	-0.3471	-0.0841
Trajectory 2	Kalman	-0.3389	-0.0838	-0.0438
	Kalman (CV)	-0.3372	-0.1013	-0.0533
	Naive	-0.6102	-0.1239	-0.1070
Trajectory 3	Kalman	-0.2341	-0.0516	-0.0357
	Kalman (CV)	-0.2200	-0.0408	-0.0270
	Naive	-0.3429	-0.1615	-0.1644

The results clearly demonstrate that the Kalman filter provides superior performance compared to the naive method. For all trajectories and sampling rates, the Kalman-based approach leads to consistently lower power losses. Notably, for Trajectory 1 at 1 Hz, the Kalman filter reduces power loss by nearly 5 times compared to the naive method, highlighting the significant benefit of using prediction in scenarios with infrequent updates.

Another consistent trend across all results is the impact of the sampling rate. As the sampling frequency increases, the power loss decreases for both methods. This is expected, as more frequent reconfiguration allows the RIS to better adapt to the UE's motion. At lower sampling rates (particularly 1 Hz), both methods suffer due to the longer intervals between updates. However, the naive approach is more severely affected, since it fully relies on outdated information and does not attempt to estimate the UE's position.

In the case of the Kalman filter, the reduced performance at lower sampling rates arises from two factors: modeling error, as the motion dynamics are less accurately captured over longer prediction horizons, and information decay, since the filter's predictions become less reliable in the absence of new measurements. This highlights the importance of both accurate motion models and timely updates in predictive tracking.

A further insight emerges when comparing the constant velocity Kalman filter to the standard Kalman filter. In scenarios involving abrupt motion changes or non-linear trajectories, such as in Trajectory 1, where the UE follows a circular path, the CV model struggles to maintain accurate tracking. Because it assumes linear motion with no acceleration, it cannot adapt to changes in speed or direction, resulting in systematic tracking errors. Specifically, it tends to lag behind during turns and overshoot when the UE slows down or stops. These inaccuracies manifest as fluctuations in received power, especially at lower sampling rates, where the time between updates exacerbates the model's limitations. Overall, the standard Kalman filter exhibits more stable and reliable performance in dynamic scenarios.

V. Conclusions and Next Research Project

This paper presents a predictive RIS control strategy based on Kalman filtering to compensate for the limited availability of high-rate UE location data. In particular, the paper addresses scenarios where the UE position is obtained from low-rate GPS updates, a common constraint in real-world deployments.

Through extensive simulations over different trajectories and sampling rates, it is demonstrated that the Kalman filter can significantly improve RIS reconfiguration performance compared to a naive update strategy. The results show up to a 5-fold reduction in average power loss at the UE. The benefit becomes more pronounced as the sampling interval increases, highlighting the predictive capability of the Kalman filter in maintaining signal alignment over longer periods without fresh measurements.

This work also compared two motion models within the Kalman filter framework: the standard CA model and the CV model. The CV model exhibits reduced accuracy during turns or abrupt motion changes, as it does not account for acceleration. This limitation is particularly evident in Trajectory 1, where the UE follows a circular path.

Notice that the Kalman filter requires careful tuning of its process and measurement noise covariance matrices to ensure satisfactory performance. Poorly chosen parameters can lead to unstable estimates or degraded tracking accuracy, especially under varying mobility conditions. Additionally, several other factors can introduce errors in Kalman filtering, including its reliance on accurate system modeling, the assumption of Gaussian noise, and the requirement for linear dynamics—all of which, when violated, can negatively impact estimation quality. Indeed, while simplifications made in modeling both the UE's movement (CV/CA models) and the radio environment (basic path-loss, isotropic antennas, ideal RIS) become the problem tractable and demonstrate the core concept effectively, they mean that the reported performance gains (e.g., "up to a fivefold improvement") should be seen as an optimistic upper bound. Real-world deployments will likely diminish gains due to more erratic UE motion, complex multipath, and hardware imperfections. Besides, the system's performance could degrade substantially due to severe GPS errors (outages, large outliers common in urban canyons) or practical RIS limitations (discrete phases, losses, switching times).

The focus on a single UE and specific trajectory types means that its direct applicability to dense, multi-user scenarios or highly diverse mobility patterns is not fully established. Hence, while the core predictive idea is sound, significant further research would be needed to scale this solution to the complexity of real B5G/6G deployments.

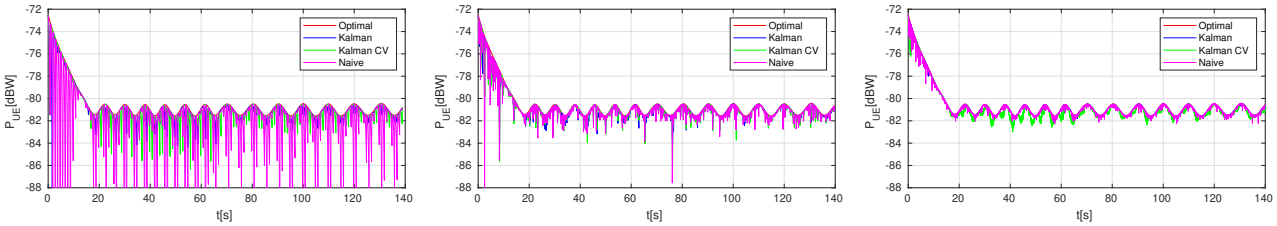

(a) 1Hz (b) 5Hz (c) 10Hz

Fig. 2. Power loss at the UE for trajectory 1 considering (a) 1Hz (b) 5Hz (c) 10Hz sampling rates

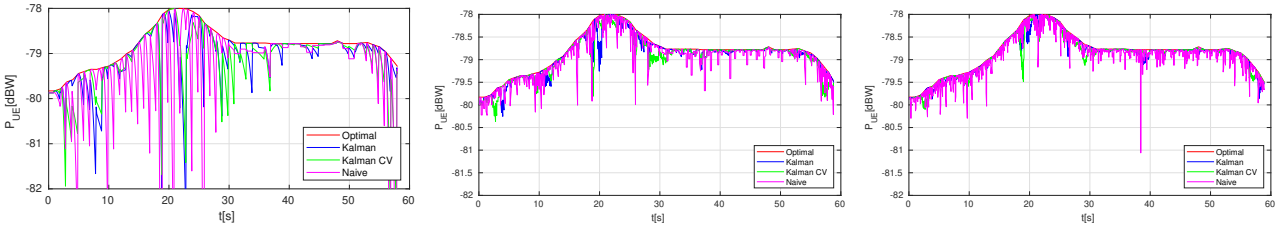

(a) 1Hz (b) 5Hz (c) 10Hz

Fig. 3. Power loss at the UE for trajectory 2 considering (a) 1Hz (b) 5Hz (c) 10Hz sampling rates

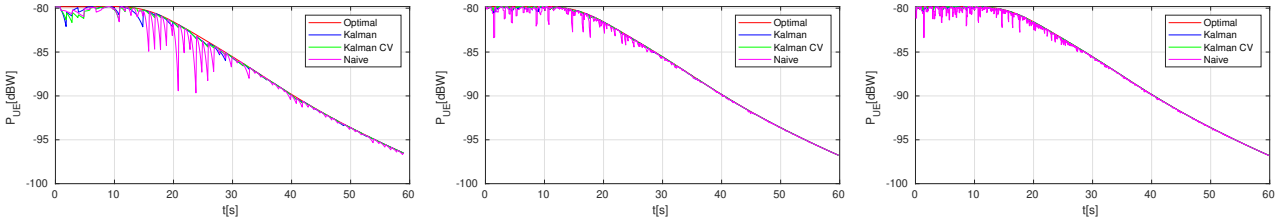

(a) 1Hz (b) 5Hz (c) 10Hz

Fig. 4. Power loss at the UE for trajectory 3 (simulated) considering (a) 1Hz (b) 5Hz (c) 10Hz sampling rates

Future work should focus on incorporating more realistic motion models and advanced state estimation techniques, such as the Interacting Multiple Model Kalman Filter (IMM-KF), which combines multiple motion models to improve tracking performance in systems with switching dynamics, or machine learning-based predictors. In parallel, more sophisticated scenarios, channel and RIS models should be considered to better reflect real-world propagation conditions.

REFERENCES

[1] M. A. ElMossallamy, H. Zhang, L. Song, K. G. Seddik, Z. Han, and G. Y. Li, "Reconfigurable intelligent surfaces for wireless communications: Principles, challenges, and opportunities," *IEEE Transactions on Cognitive Communications and Networking*, vol. 6, no. 3, pp. 990–1002, 2020.

[2] Z. Chen, G. Chen, J. Tang, S. Zhang, D. K. So, O. A. Dobre, K.-K. Wong, and J. Chambers, "Reconfigurable-intelligent-surface-assisted B5G/6G wireless communications: Challenges, solution, and future opportunities," *IEEE Communications Magazine*, vol. 61, no. 1, pp. 16–22, 2023.

[3] Y. Liu, X. Liu, X. Mu, T. Hou, J. Xu, M. Di Renzo, and N. Al-Dhahir, "Reconfigurable intelligent surfaces: Principles and opportunities," *IEEE Communications Surveys & Tutorials*, vol. 23, no. 3, pp. 1546–1577, 2021.

[4] S. A. Abdel Hakeem, H. H. Hussein, and H. Kim, "Vision and research directions of 6G technologies and applications," *Journal of King Saud University - Computer and Information Sciences*, vol. 34, no. 6, Part A, pp. 2419–2442, 2022. [Online]. Available: https://www.sciencedirect.com/science/article/pii/S1319157822001033

[5] J. He, H. Wymeersch, T. Sanguanpuak, O. Silven, and M. Juntti, "Adaptive beamforming design for mmWave RIS-aided joint localization and communication," in *2020 IEEE Wireless Communications and Networking Conference Workshops (WCNCW)*, 2020, pp. 1–6.

[6] Z. Zhang, T. Jiang, and W. Yu, "Active sensing for localization with reconfigurable intelligent surface," in *ICC 2023 - IEEE International Conference on Communications*, 2023, pp. 4261–4266.

[7] Y. He, Y. Cai, H. Mao, and G. Yu, "RIS-assisted communication radar coexistence: Joint beamforming design and analysis," *IEEE Journal on Selected Areas in Communications*, vol. 40, no. 7, pp. 2131–2145, 2022.

[8] M. Fabiani, D. Silva, A. Abdallah, A. Celik, and A. M. Eltawil, "Multimodal sensing and communication for V2V beam tracking via camera and GPS fusion," in *2024 58th Asilomar Conference on Signals, Systems, and Computers*, 2024, pp. 1–6.

[9] F. T. Mariotto, N. B. Yoma, and M. C. d. Almeida, "Unsupervised competitive learning clustering and visual method to obtain accurate trajectories from noisy repetitive GPS data," *IEEE Transactions on Intelligent Transportation Systems*, vol. 26, no. 2, pp. 1562–1572, 2025.

[10] S. Särkkä, *Bayesian Filtering and Smoothing*, ser. Institute of Mathematical Statistics Textbooks. Cambridge University Press, 2013.

[11] A. P. A. Mohinder S. Grewal, *Kalman filtering: Theory and practice using MATLAB*, 3rd ed. Wiley-IEEE Press, 2008.

[12] P. Y. C. H. Robert Grover Brown, *Introduction to Random Signals and Applied Kalman Filtering, Third Edition*, 3rd ed. John Wiley & Sons, 1996.

[13] U. Onyekpe, V. Palade, S. Kanarachos, and A. Szkolnik, "IO-VNBD: Inertial and odometry benchmark dataset for ground vehicle positioning," *Data in Brief*, vol. 35, p. 106885, 2021. [Online]. Available: https://www.sciencedirect.com/science/article/pii/S2352340921001694

[14] C. Hull, "1Hz GPS tracking data," 2024. [Online]. Available: https://data.mendeley.com/datasets/xt69cnwh56/3

[15] F. Costa and M. Borgese, "Electromagnetic model of reflective intelligent surfaces," *IEEE Open Journal of the Communications Society*, vol. 2, pp. 1577–1589, 2021.